

TUNING THE SUPERCONDUCTING LINAC AT LOW BEAM INTENSITIES*

N. R. Lobanov[#], P. Linardakis and D. Tsifakis, The Department of Nuclear Physics, Research School of Physics and Engineering, The Australian National University, Canberra, Australia

Abstract

The ANU Heavy Ion Accelerator Facility (HIAF) is comprised of a 15 MV electrostatic accelerator followed by a superconducting linac booster. Employment of double terminal stripping allows the system to accelerate beams with mass up to 70 amu. The disadvantage of double terminal stripping is low beam intensity of few particle nanoamps delivered to the linac. One of the linac set up procedures developed at ANU utilises a U-bend at the end of the linac. One special wide Beam Profile Monitor (BPM) is installed after the 90 degree magnet. The technique allows correct setting of phase by observing the displacement of beam profile versus phase shift of the last phase locked resonator. In this paper, a simple method has been proposed to improve sensitivity of a commercially available BPM for efficient operation with low beam intensities. Verification of BPM with enhanced sensitivity is accomplished during routine linac operations and it is supplemented by longitudinal phase space simulations.

INTRODUCTION

The ANU Heavy Ion Facility (HIAF) is comprised of a 15 MV electrostatic accelerator followed by a superconducting linac booster as shown in Fig. 1 [1]. A pulsed beam is obtained using a single frequency grid buncher operating at 1/16th sub-harmonic of the linac frequency of 150 MHz and positioned at low energy (LE) of the 14UD accelerator. The beam bunches have a typical pulse width of 1.5 ns FWHM with a bunching efficiency ~25%. The beam is further compressed to ~ 100 ps wide by the superconducting buncher “C1” made up of a $\beta=v/c=0.1$ Quarter Wave Resonator (QWR).

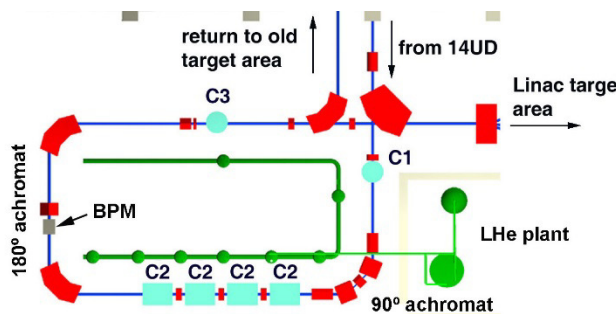


Figure 1: Layout of the ANU superconducting linac booster. The main components are: the superbuncher C1; split loop resonator modules C2 and the time-energy lens C3. Bending radius of 180° achromat dipole is $R_{180^\circ} = 1100$ mm. The distance from exit of 180° achromat dipole to large bore BPM is $L=1608$ mm.

The twelve, $\beta=0.1$, lead tin electroplated resonators currently installed in module cryostats “C2” mean that only double terminal stripped ions from the 14UD with mass below ~70 amu match adequately the resonator gap separation. Heavier ions have velocity at injection into the linac of $\beta < 0.06$, limiting its performance due to TTF mismatching. The Time-Energy Lens (TEL), a $\beta=0.1$ QWR, “C3”, serves as the energy homogenizer for return of the beam to the old target area or as rebuncher for optimal time resolution. Two main factors limit 14UD performance due to double terminal stripping operation: limited beam intensity and range of beams available from the ion sources and restriction on transmission and significant loading associated with heavy beams. For example, the beam loading limits the maximum intensity of injected beams to 1.5 μ A at LE end. Typically, with double terminal stripping and single frequency bunching, one can produce nanoamp beams injected into the linac. Specialised, sensitive equipment is required to tune linac with such low intensity beams.

The setting of the bunching and acceleration phase of the resonators can be achieved by a few different techniques. First, it can be done by interpreting the BPM trace in the middle of the 180 degree achromat [2]. The energy dispersion at this location allows observation of the beam energy affected by each successive resonator. The second technique employs a fast Faraday cup, which provides a direct view of the time structure of the beam [3]. More sophisticated application employs a superconducting resonator to detect the arrival time of a beam bunch [4].

This paper has been organised into three main sections. The first section outlines the general concept of a BPM with factor of 2.5 increased sensitivity and describes resonator set up procedures. The second section presents key experimental results based on new techniques, including using a high sensitivity BPM to set up linac resonators for effective acceleration. Finally, the third section presents interpretation of linac tune results and defines technique limitations.

METHODS

A beam profile is generated by collecting secondary electrons that are produced when rotating wire intersects the beam. The scanner element is made of 1.5 mm diameter molybdenum wire. With the axis of rotation of the wire inclined at 45° to the vertical, it scans the beam twice in each cycle at 19 Hz in the horizontal and vertical directions. An isolated cylindrical electrode mounted coaxially with the housing collects secondary electrons released from the wire. The collector is coupled electrically

*Work supported by Heavy Ion Accelerators Education Investment Fund
[#]Nikolai.Lobanov@anu.edu.au

to a sensitive current amplifier with an adjustable gain up to 10^8 V/A. It is sensitive to beam currents of a few nanoamps.

Assuming a round beam with radius r and a symmetric Gaussian particle density distribution in both transverse directions $j(x,y)$, the measured beam profile in x plane $I(x)$ can be represented by the integral equation $I(x) = \delta \eta_{coll} \int j(x,y) dy$, where δ accounts for the secondary emission coefficient of the wire and η_{coll} is the efficiency of the electron collection system. The δ ranges from few to few hundred and depends on the material of the wire and the energy and atomic number of the incident ion. A molybdenum wire is a good material choice as it has both high δ coefficient and low sputter yield.

The η_{coll} depends on the wire diameter and geometry of collector housing. A wire diameter larger than 1.5 mm will limit achievable spacial resolution. An aperture at the entrance flange of the collector shields against direct interception of a widely divergent ion beam. Some secondary electrons might escape the collector surface through those openings. Since most of the emitted secondary electrons are in the energy region below 200 eV, a bias voltage of about +300 V is sufficient to suppress it.

A DC-blocking capacitor is used to connect the collector to the preamplifier, such that only the AC signal from the collector can pass through while the DC bias voltage is blocked as shown in Fig. 2.

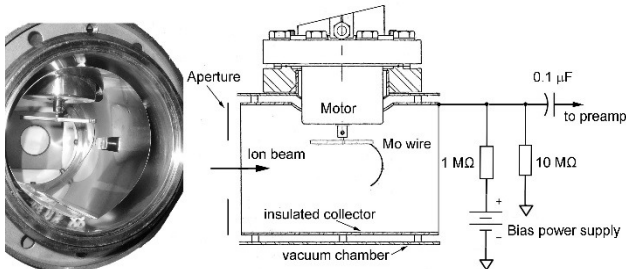


Figure 2: Image of NEC BPM with its schematic cross-section, collector bias circuit and DC-blocking filter capacitor circuit to filter out AC bias signal in BPM electronics set up.

Capacitive coupling has the disadvantage of degrading the low frequency performance of BPM electronic devices. The coupling capacitor along with the input electrical impedance of the preamplifier forms a high-pass filter. So for adequate low frequency response, the capacitor should have a capacitance value $C \sim 0.1 \mu\text{F}$, such that its reactance is at most a tenth of the input impedance of preamplifier at the lowest frequency of interest.

Figure 3 presents an example of two sets of observed $^{12}\text{C}^{+5}$ 70 MeV 10 nA beam profiles obtained with a biased and unbiased collector. The measured rms noise level in BPM electronic system is typically $U_{N_{rms}} \sim 80$ mV. An acceptable signal to noise ratio (SNR) should be higher than 1:1 in order to isolate a desired signal U_S from noise floor U_N . For a 70 MeV $^{12}\text{C}^{+5}$ beam, the minimum resolved beam current when operating with the unbiased BPM

collector is $I_{unbiased} = 10 \text{ nA} \times 80 \text{ mV}/1000 \text{ mV} = 0.8 \text{ nA}$, assuming that the beam cross section does not change with the current. The collector signal is proportional to the secondary electron emission coefficient, δ , of the rotating wire. Application of a bias voltage to the collector increases resolution by a factor of 2.1, pushing down the minimum measured beam current to $I_{biased} = 0.38 \text{ nA}$. This is similar to phase detection with a superconducting cavity [5].

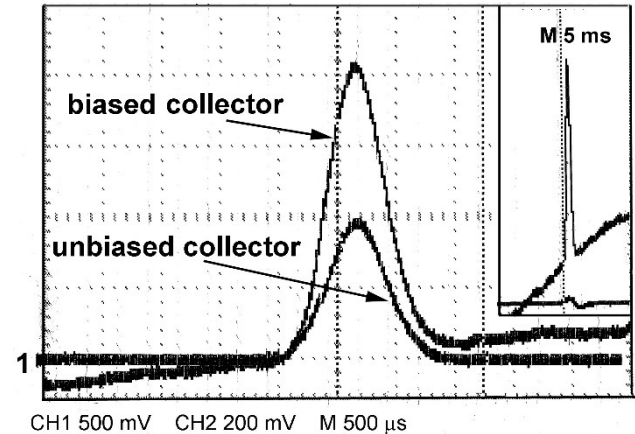


Figure 3: $^{12}\text{C}^{+5}$ beam horizontal X profiles produced with biased and unbiased BPM collector (top traces "1"). The single stripped beam energy is 70 MeV and beam current 10 nA. Bias voltage +300 V. Beam current of 10 nA has generated voltage distribution with 1 V maximum at BPM preamp gain of 10^8 V/A with unbiased collector and 2.1 V with collector biased. The inset shows the modulation of induced current in the rotating wire with the frequency corresponding to 1140 RPM of BPM motor. Note different time scale in the inset image.

All linac tunes are undertaken by interpreting the BPM trace in the middle of 180° achromat using a special large bore BPM83. The energy dispersion by each successive resonator causes the beam position displacement ΔX_{BPM} in horizontal X direction according to low angle approximation expression:

$$\Delta X_{BPM} \approx 0.5(R_{180^\circ} + L)\Delta E/E_0, \quad (1)$$

where $R_{180^\circ} = 1100$ mm is the bending radius of the 180° achromat dipole; $L = 1608$ mm is the distance from exit of the 180° achromat dipole to BPM; ΔE is the energy gain/loss introduced by the resonator which is currently being tuned and E_0 is the beam energy. The analysis of the motion of the BPM's helical wire through the beam leads to a calibration distance, d , between fiducial marks according to the equation $d = \pi r / \sqrt{2} = 11.8$ cm, where $r = 5.31$ cm is the scanning circle radius. The conversion of oscilloscope time axis ΔT_{osc} [ms] into a horizontal distance is given by the formula $\Delta X_{BPM} [\text{cm}] = d \Delta T_{osc} / \tau_f$, where $\tau_f = 33$ ms is the time interval between two fiducial signals

displayed on an oscilloscope. The energy gain/loss is calculated by:

$$\Delta E = QE_{\text{acc}} L_{\text{SLR}} \sin(\Delta\Psi) T_{(\beta)}, \quad (2)$$

where Q is the ion beam charge state; $E_{\text{acc}}=3$ MV/m is an average accelerating field at 6 W; $L_{\text{SLR}}=0.221$ m is the active length of the SLR; $\Delta\Psi$ is the resonator field phase deviation from 0° (crossover phase) and transit time factor $T_{(\beta)}=1$ for ions with optimum velocity $\beta=0.1$. Small phase magnitudes approximate to $\sin(\Delta\Psi)\approx\Delta\Psi$. Therefore, after combining equations (1), (2) and substituting ΔX_{BPM} with ΔT_{osc} one can derive the expression:

$$\Delta\Psi[\text{rad}] = 7.2 E_0 \Delta T_{\text{osc}} / ((R_{180^\circ} + L) Q E_{\text{acc}} L_{\text{SLR}} T_{(\beta)}) \quad (3)$$

From Fig. 3, the oscilloscope time resolution, ΔT_{min} , is about 0.2 ms. Assuming typical values for $E_0=270$ MeV and $Q=20$, the BPM phase resolution can be estimated from (3) as $\Delta\Psi_{\text{min}}=0.6^\circ$. Higher phase resolution can be achieved using a superconducting SLR in phase detection mode as described in [5].

RESULTS

Validation of the new technique was accomplished during routine linac tunes when accelerating $^{48,50}\text{Ti}^{+17}$, $^{50,52,54}\text{Cr}^{+18}$, $^{64}\text{Ni}^{+19}$ and $^{40}\text{Ca}^{+16}$ ions, with the all beams used for a physics experiment. All beams were produced using a $4 \mu\text{g}/\text{cm}^2$ carbon foil in the terminal (TS) of the 14UD and the second Linac Stripper (LS) $12 \mu\text{g}/\text{cm}^2$ foil with the exception of $^{64}\text{Ni}^{+19}$, which was produced with Double Terminal Stripping (DTS). With DTS the Ni beam was initially stripped to charge state $Q_1=12$ using a $4 \mu\text{g}/\text{cm}^2$ carbon foil in the terminal and the final charge state with $Q_2=19$ with the second terminal $8 \mu\text{g}/\text{cm}^2$ carbon foil stripper. Determination of the bunching and acceleration phase of the QWRs and SLRs was done by interpreting the BPM trace as described in the previous section. The energy dispersion at this location allowed observation of the energy of the beam as it was affected by each successive resonator. The crossover phase and its type, 0 or 180° , was inferred by variation of the resonator phase from $\pm 180^\circ$. The acceleration phase was set at -18° with respect to the maximum acceleration phase for phase stability. An unwelcome by-product was over-bunching which was evidenced by a wide BPM trace, equivalent to a wide energy spread. To counteract this, the acceleration phase was set to $+18^\circ$ when this lead to an improvement in beam profile. Typically this was necessary in 1 cavity across the entire linac. The energy gain of the accelerated beam was determined by scaling the magnetic field in the first dipole of the 180° achromat.

All cavities were tuned and set for acceleration using standard BPM-based techniques and a BPM with improved sensitivity when operating with low beam intensity. A summary of operation conditions corresponding to two selected linac tunes is listed in the Table 1.

Table 1: Comparison of Linac Tunes Based on BPM Techniques

SLR	250 MeV DTS $^{64}\text{Ni}^{+19}$			186 MeV TS+LS $^{52}\text{Cr}^{+18}$		
	E_{acc} , MV/m	β	ΔE , MeV	E_{acc} , MV/m	β	ΔE , MeV
1.1	2.51	0.093	9.9	2.50	0.089	9.2
1.2	2.70	0.095	10.7	2.56	0.091	9.5
1.3	2.66	0.096	10.6	2.59	0.093	9.7
2.1	1.94	0.098	7.8	1.98	0.095	7.5
2.2	1.97	0.099	7.9	1.95	0.097	7.4
2.3	2.25	0.101	9.0	2.11	0.098	8.0
3.1	2.20	0.102	8.8	2.29	0.1	8.7
3.2	2.60	0.104	10.4	2.59	0.102	9.8
3.3	2.48	0.105	9.9	2.58	0.104	9.8
4.1	1.97	0.106	7.8	2.00	0.105	7.5
4.2	2.06	0.108	8.1	2.07	0.107	7.8
4.3	1.18	0.108	4.7	1.13	0.108	4.2

In Table 1, the identification of resonators is by numbering 1.1, 1.2, 1.3, 2.1, ..., 4.3, where the first number categorizes one of the four module cryostats and the second number is one of the three SLRs contained in each module cryostat. The first tune is the acceleration of $^{64}\text{Ni}^{+19}$ produced with DTS from initial energy of 250 MeV to ~ 355 MeV. In the terminal, the Ni beam was initially stripped to charge state $Q_1=12$. The second tune is the acceleration of $^{52}\text{Cr}^{+18}$ produced with TS and LS from initial energy of 186 MeV to ~ 285 MeV. The energy gain/loss is calculated according to the formula $\Delta E = Q_2 E_{\text{acc}} L_{\text{SLR}} \cos(\phi) T_{(\beta)}$, where Q_2 is the ion beam charge state after the 2nd stripper; $E_{\text{acc}}=2\div 3$ MV/m is an average accelerating field; $L_{\text{SLR}}=0.221$ m is the active length of the SLR; $\phi = -18^\circ$ is the resonator accelerating phase and transit time factor $T_{(\beta)}=1$ for ions with optimum velocity $\beta=0.1$. The quality of linac tunes is judged on the following: beam transmission through the linac and up to the target devices, the energy gain, transverse dimension and pulse width/energy spread in specified measurement locations. Figure 4 shows transformation of longitudinal phase space ellipses for both tunes simulated with SPACE code through the injection section of the linac, consisting of a superbuncher and 90° achromatic bend up to the first linac SLR.

Pulsed beams are obtained using single frequency, single gap grid buncher positioned at low energy of the 14UD. The beam bunches used in SPACE simulations have a pulse width of 1.0 ns FWHM and calculated FWHM energy spread of 128.3 keV for $^{64}\text{Ni}^{+19}$ and 98.7 keV for $^{52}\text{Cr}^{+18}$, shown in Fig. 4 as an ellipse without fill. The beam is further compressed to <100 ps wide at the first resonator in the linac, 1.1 (yellow ellipse), by the superconducting buncher $\beta=0.1$ QWR operating at 0.5 – 0.6 MV/m and introducing an energy gain to the incoming beam. The bunching action of the superbuncher is shown as an ellipse with green fill in Fig. 4.

The first step of linac tuning is the determination of the correct bunching phase of the superbuncher QWR operating at nominal calculated bunching electrical field. The BPM profiles of a 2.25 nA 186 MeV $^{52}\text{Cr}^{+18}$ beam during superbuncher crossover search are shown in Fig. 5. The beam profile shown in grey colour is the pulsed beam

injected to the superbuncher from the 14UD with the peak amplitude scaled down by factor of 1/5.

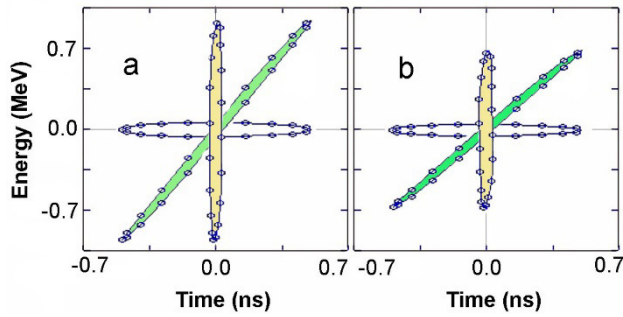


Figure 4: SPACE simulated longitudinal phase ellipses through the superbuncher to the first linac SLR 1.1: a) 250 MeV $^{64}\text{Ni}^{+19}$ DTS beam injected to superbuncher from 14UD operating with low energy pulsing system with calculated FWHM energy spread 128.3 keV and assumed time spread 1 ns; b) 186 MeV $^{52}\text{Cr}^{+18}$ TS+LS beam with FWHM energy spread 98.7 keV and time spread 1 ns. Longitudinal phase ellipse of injected pulsed beam from 14UD is without fill. Phase ellipses transformed by superbuncher QWR operating at nominal bunching field 0.62 MV/m for Ni beam and 0.47 MV/m for Cr beam are filled with green background. Beam arriving at the linac entrance to the first accelerating SLR 1.1 positioned 6.98 m away from superbuncher is described by time focus phase ellipse filled with yellow colour.

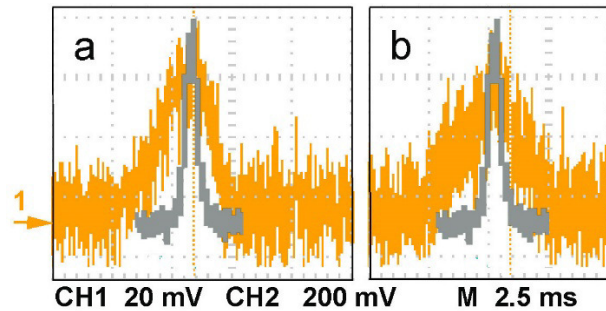


Figure 5: BPM profiles of a 2.25 nA 186 MeV $^{52}\text{Cr}^{+18}$ beam during superbuncher crossover search. Superbuncher QWR operates at nominal bunching electric field of 0.47 MV/m to produce time focus at the 1st accelerating resonator 1.1: a) crossover $+90^\circ$, b) crossover -90° . The beam profile shown in grey colour corresponds to pulsed beam with superbuncher turned off. Its amplitude is scaled down by 1/5 for clarity.

From Fig. 5, the FWHM horizontal width of the 186 MeV $^{52}\text{Cr}^{+18}$ injected beam is $\Delta X_{\text{inj}}=2.7$ mm. The FWHM horizontal width of the superbunched beam is $\Delta X_{+90^\circ}=9.2$ mm (crossover $+90^\circ$) and $\Delta X_{-90^\circ}=9.6$ mm (crossover -90°) correspondingly. The energy spread produced by superbuncher is calculated by:

$$\Delta E_{\text{SB}}=2QE_{\text{acc}}L_{\text{QWR}}\sin(\pi f\tau_{\text{inj}})T_{(\beta)}, \quad (4)$$

where Q is the ion beam charge state; E_{acc} is accelerating field required to produce time focus 6.98 m further down; L_{QWR} the active length of the QWR; f is the linac frequency; τ_{inj} is the time spread of the injected beam and transit time factor $T_{(\beta)}$, which is unity for ions with optimum velocity $\beta=0.1$. For $Q=18$, $E_{\text{acc}}=0.47$ MV/m, $L_{\text{QWR}}=0.18$ m, $f=150 \times 10^6$ Hz, $\tau_{\text{inj}}=10^{-9}$ s and $T_{(\beta)}=0.98$, the calculated energy spread is $\Delta E_{\text{SB}}=1.38$ MeV, which is consistent with the result obtained with SPACE code simulation shown in Fig. 4 (b). The energy spread ΔE_{SB} causes the beam position dispersion ΔX_{SB} in the horizontal X direction at the BPM location. ΔX_{SB} can be calculated using expression (1). For $E_0=186$ MeV, the calculated horizontal dimension of the beam is $\Delta X_{\text{SB}}=10$ mm, which is also consistent with BPM images shown in Fig. 5.

The linac tune results for crossover search and consequent setting of acceleration phase for the first two linac resonators are shown in Fig. 6.

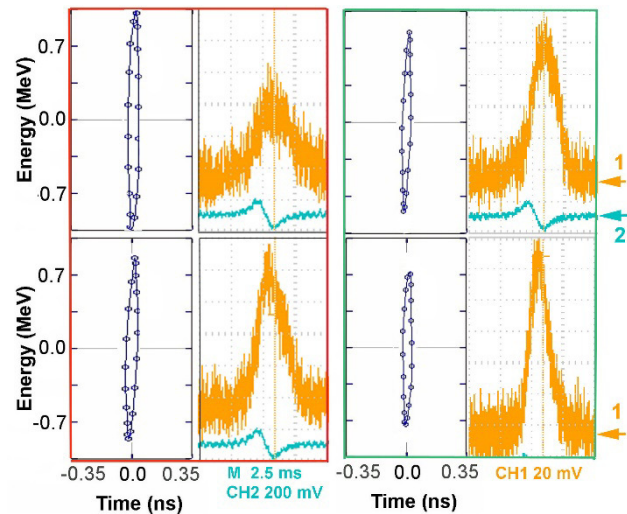


Figure 6: BPM profiles and SPACE-simulated profiles for SLR 1.1 (left square box with red border) and SLR 1.2 (right square box with green border) operating at -90° type crossover (top images) and at accelerating phase -18° (bottom images). Injected beam is 2.25 nA $^{52}\text{Cr}^{+18}$ at 186 MeV. The energy gain introduced by the resonators SLR 1.1 and SLR 1.2 is 9.2 MeV and 9.5 MeV respectively.

The ion beam injected to the linac is the same as described in the previous paragraph. BPM profiles and SPACE-simulated longitudinal phase ellipses for SLR 1.1 are enclosed in a box with red border. Images enclosed in a box with green border are taken for SLR 1.2. Top images correspond to operation of resonator at nominal field and -90° crossover phase ϕ_{-90° and the bottom images are produced for resonators running at accelerating phase $\phi_{-18^\circ}=-18^\circ$. The ratio of accelerating field derivatives at crossover and accelerating phases is given by $\sin(90^\circ)/\sin(18^\circ)=3.2$. Therefore, the energy spread introduced to the bunch during operation of the resonator at crossover phase is higher than at accelerating phase as seen in Fig. 6 by comparing corresponding phase ellipses.

In addition, higher energy spread results in a wider BPM trace at ϕ_{-90° (top images in Fig. 6) as compared to ϕ_{-18° (bottom images).

An over-bunching is evidenced by a wide BPM trace equivalent to a wide energy spread as shown in Fig. 7 (a). To counteract this, the acceleration phase of the selected resonator is set to $+18^\circ$ when this leads to an improvement in beam profile, Fig. 7 (b).

The cumulative energy spread introduced by the superbuncher and resonators, ΔE_{SB+RES} , causes the beam position dispersion ΔX_{SB+RES} in the horizontal X direction at the BPM location. Typically, ΔE_{SB+RES} varies along the linac around ΔE_{SB} due to particle phase oscillations. From Fig. 7, the FWHM horizontal width of the 250 MeV $^{64}\text{Ni}^{+19}$ beam injected into the linac is $\Delta X_{inj}=2.1$ mm. The FWHM horizontal width of 318 MeV beam boosted with seven linac resonators from 1.1 to 3.1 is $\Delta X_{+18^\circ}=8.9$ mm at $\phi_{acc}=+18^\circ$ and $\Delta X_{-18^\circ}=2.8$ mm at $\phi_{acc}=-18^\circ$ correspondingly. Overbunching caused by SLR 3.1 introduces excessive energy spread ΔE_{SB+RES} , manifested in a wide horizontal beam width ΔX_{-18° as shown in Fig. 7(a). To overcome this problem, accelerating phase of SLR 3.1 is advanced by 36° to $+18^\circ$ in order to preserve high beam transmission through the linac, Fig. 7 (b).

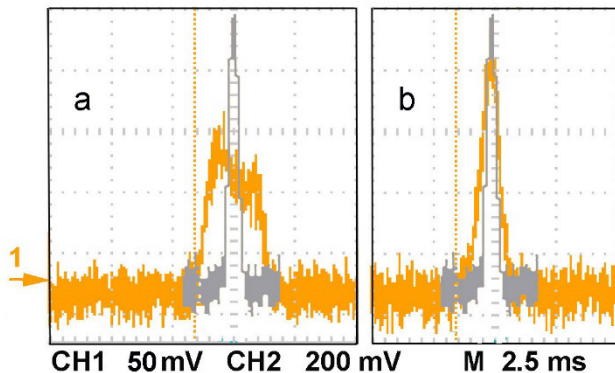


Figure 7: BPM profiles of 1.5 nA 318 MeV $^{64}\text{Ni}^{+19}$ beam boosted with seven linac resonators from 1.1 to 3.1. All resonators operate at nominal accelerating field and phases -18° as listed in a Table: a) SLR 3.1 accelerating phase is -18° , b) SLR 3.1 accelerating phase is advanced by $+36^\circ$ to $\phi_{acc} = +18^\circ$ to overcome the effect of over-bunching. The beam profile shown in grey colour corresponds to pulsed beam with superbuncher and all linac resonators turned off.

DISCUSSION

BPM phase resolution can be estimated from (3) as $\Delta\Psi_{min}=0.6^\circ$. Higher phase resolution can be achieved using superconducting SLR in phase detection mode as described in [5]. However, the high precision ϕ_{acc} setting does not result in higher beam energy gain or transmission as demonstrated in [5]. BPM tuning technique with collector bias allows better sensitivity to accelerating current when compared to the unbiased case. The minimum estimated resolved beam current when operating with the unbiased

BPM collector is 0.8 nA, which is consistent with the BPM profile for $^{52}\text{Cr}^{+18}$ beam shown in Fig. 5. Application of a bias voltage to the collector pushes down the minimum measured beam current to ~ 0.38 nA. This is particularly important when tuning low intensity beams through the superbuncher and first few linac resonators.

In a biased BPM, the rotating wire periodically passes through a variable electrical field. As a result, the induced charge on the wire is modulated with the frequency corresponding to 1140 RPM of the BPM motor as shown in the inset of Fig. 3. This current modulation does not greatly affect the shape of beam profile, but rather the base line. If required, the modulation can be suppressed by improved shielding of the collector.

The BPM profiles observed during determination of the correct bunching and acceleration phases are dominated by the energy spread of the beam bunches, which causes the widening of the horizontal width of the beam as shown in Fig. 5 and 6. Looking at the shapes and width of the BPM profile allows determination of whether the longitudinal phase ellipse is evolving within the optimum constraints. When over-bunching is observed, which is evidenced by a wide BPM trace equivalent to a higher energy spread and poor transmission (Fig. 7), the acceleration phase is set to $+18$ degrees in a selected resonator when this leads to an improvement in the beam profile. Typically, this is necessary in the first or second resonator of the third cryostat SLR 3.1.

The BPM tuning technique provides good accuracy to determine the bunch arrival time and setting bunching and acceleration phases. The BPM technique with improved sensitivity due to bias improves overall operation capability, resulting in considerable enhancement in linac performance and its availability for operation with low beam intensity.

ACKNOWLEDGEMENT

This work has been supported by Australian Federal Government Superscience/EIF funding under the NCRIS mechanism.

REFERENCES

- [1] D.C. Weisser, and N.R. Lobanov, Linac Boosters – An Overview, Amer. Inst. of Phys. Conf. Proc. 473 (ed. K. Shepard) (1999) 117-137.
- [2] S. Canella, in Proceedings of the 1997 International Conference on Accelerator and Large Experimental Physics Control Systems, Beijing, China (1997), p.491
- [3] M. Bellato, A. Dainelli, M. Poggi, Nucl. Instr. And Meth. In Phys. Res. A 382 (1996) 118-120.
- [4] S.I. Sharamentov, R.C Pardo, P.N. Ostroumov et all, Phys. Rev. ST Accel. Beams, 6, 052802 (2003).
- [5] N. R. Lobanov, P. Linardakis and D. Tsifakis, "Tuning the linac with superconducting resonator used as a phase detector", Proc. SRF2015, <http://jacow.org/>